Sea-ice evaluation of NEMO-Nordic 1.0: a NEMO–LIM3.6 based ocean–sea ice model setup for the North Sea and Baltic Sea

Per Pemberton[1], Ulrike Löptien[3], Robinson Hordoir[2], Anders Höglund[2], Semjon Schimanke[2], Lars Axell[2], and Jari Haapala[4]

[1]Swedish Meteorological and Hydrological Institute, 426 71 Gothenburg, Sweden
[2]Swedish Meteorological and Hydrological Institute, 601 76 Norrköping, Sweden
[3]GEOMAR Helmholtz Centre for Ocean Research Kiel, Düsternbrooker Weg 20, 24105 Kiel, Germany
[4]Finnish Meteorological Institute, FI-00101 Helsinki, Finland

Correspondence to: Per Pemberton
(per.pemberton@smhi.se)

Abstract. The Baltic Sea is a seasonally ice covered marginal sea in northern Europe with intense wintertime ship traffic and a sensitive ecosystem. Understanding and modeling the evolution of the sea-ice pack is important for climate effect studies and forecasting purposes. Here we present and evaluate the sea-ice component of a new NEMO–LIM3.6 based ocean–sea ice setup for the North Sea and Baltic Sea region. The setup includes a new depth-based fast ice parametrization for the Baltic Sea. The evaluation focuses on long-term statistics, from a 45-year long hindcast, although short-term daily performance is also briefly evaluated. Different sea-ice metrics such as sea-ice extent, concentration and thickness are compared to the best available observational dataset to identify model biases. Overall the model agrees well with the observations in terms of the long-term mean sea-ice extent and thickness. The variability of the annual maximum Baltic Sea ice extent is well in line with the observations but the 1961–2006 trend is underestimated. Based on the simulated ice thickness distribution we estimate the undeformed and deformed ice thickness and concentration in the Baltic Sea, which compares reasonably well with observations. We conclude that the new North Sea/Baltic Sea ocean–sea ice setup is well suited for further climate studies and sea ice forecasts.

1 Introduction

The Baltic Sea is seasonally ice covered and in the northern part the sea-ice season can last for up to 7 months. The maximum total sea-ice extent is usually reached in late February and between mid-February and mid-March the ice covers on average 45% of the total Baltic Sea area. However, interannual fluctuations around this mean are very large and the ice extent can reach a coverage of almost 100% during severe winters (Leppäranta and Myrberg, 2009; Vihma and Haapala, 2009).

With 15% of the world's cargo transportation, the Baltic Sea is one of the heaviest trafficked seas in the world (HELCOM, 2009). Despite the harsh wintertime sea-ice conditions intense maritime traffic proceeds through-out the year with ships continuously operating to the northernmost ports of the Baltic Sea. This usually requires some assistance by ice-breakers and traffic restrictions based on the ship's ice class are therefore imposed by the ice-breaking authorities (HELCOM, 2004).

Regular sea-ice forecasts are thus vital to support the intense ship traffic and numerical ocean–sea ice models together with satellite and ship-based observations are used by the operational Ice Services around the Baltic Sea. Here not only the extent of the ice cover is of interest, but also ice thickness and information about the ice types are highly relevant. Close to the coasts and in shallow areas the ice usually appears as fast ice while it is drifting elsewhere (Leppäranta and Myrberg, 2009). As a

5 consequence of surface and bottom stresses, due to winds and ocean currents, convergent ice motion can lead to deformations of the ice pack. This creates so called ice ridges, barriers of very thick ice, which can be up to 30 m thick (Leppäranta and Myrberg, 2009). In addition, a convergent ice field can lead to high ice pressure that can severely hinder the ice-going traffic. It is therefore of high importance for the maritime traffic to monitor and forecast the extent of ridged ice and ice pressure (Leppäranta and Hakala, 1992; Löptien et al., 2013).

10 In addition, results from sea-ice models have also been used for understanding winter maritime traffic and analyzing winter ship navigation accidents (Goerlandt et al., 2016), building a winter navigation risk model (Valdez Banda et al., 2015), and developing data-driven models for ship performance in ice (Montewka et al., 2015).

For the climate system sea ice constitutes a barrier that strongly reduces the exchange of heat, nutrients and gases as well as impacts the momentum transfer between the ocean and atmosphere. Here numerical ocean–sea ice models have been used as

15 the main tool to understand how changes in the climate system would impact the state of the Baltic Sea (Haapala et al., 2001; Meier, 2006), how changes in the ice cover affects biogeochemistry (Eilola et al., 2013) and how changes in sea ice impacts Baltic ringed seals (Meier et al., 2004).

Clearly the need to model sea-ice processes is an integral part of the ocean–sea ice forecasting task, crucial for maritime winter traffic studies as well as an important component of the coupled ocean–ice–atmosphere climate system. Even though the

20 physical processes at work are the same on these different time and spatial scales, model limitations have called for different models systems to be used at the Swedish Meteorological and Hydrological Institute (SMHI) in the past for ocean–sea ice forecasting (Funkquist and Eckhard Kleine, 2007) and climate studies (Meier et al., 2003) of the Baltic Sea. The development of such models is time consuming and a common model system would thus be beneficial. Here the use of a community model system such as e.g. NEMO (Nucleus for European Modelling of the Ocean) (Madec, 2016) provides an excellent tool to

25 keep up with the state-of-the-art model development. This approach has been adopted at SMHI where a new NEMO-based configuration – NEMO-Nordic – used both for forecasting and climate purposes, has been setup for the Baltic and North seas.

The scope of this article is to present the sea-ice component of NEMO-Nordic to the community. This is done by evaluating a 45-year long hindcast simulation of the Baltic Sea with a set of observations. The article is outlined as follows: in section 2 we describe the model, simulation, metrics and observational data set that are used. In section 3 we evaluate the new configuration

30 focusing on the 45-year long hindcast simulation, followed by a summary and conclusions in section 4. Note that the ocean component of NEMO-Nordic is presented and evaluated in Hordoir et al. (2015) and in a forthcoming separate article (Hordoir et al., A NEMO based ocean model for Baltic & North Seas, research and operational applications; in preparation).

2 Methods

2.1 Model Description

The model framework NEMO and the integrated Louvain-la-Neuve sea ice model (LIM) provides possibilities to simulate ocean and sea ice processes on a multitude of time and space scales with applications ranging from global climate simulations to regional forecasts. Here we describe our NEMO-Nordic setup that uses the stable NEMO-LIM3 version 3.6 in a regional configuration covering the North and Baltic seas. Below we briefly describe the different components of the configuration with the specific choices of parameter settings and physics options.

2.1.1 The Ocean Model

The main model domain of NEMO-Nordic covers the English Channel, North Sea and Baltic Sea. In the present study we use a sub-region of the main domain covering only the Baltic Sea and Kattegat to save computational time. This setup has the same physical options, horizontal and vertical resolutions as the larger North Sea/Baltic Sea domain. The only difference is that the open boundary is in Kattegat instead of in the English Channel and the North Sea. The effect of omitting the Skagerrak and North Sea region is very limited for the Baltic Sea ice state as the sea-ice growth and melt is mainly driven by the surface fluxes rather than the advective signal. However, sea-ice can occasionally form along the Swedish west coast in the Skagerrak region and this is obviously not simulated in this setup.

NEMO-Nordic's horizontal resolution is 0.055° in the zonal and 0.033° in the meridional direction. This amounts to a nominal resolution of 3.7 km (2 nautical miles). Compared to the first baroclinic Rossby radius, which is 2–11 km in the Baltic Sea (Alenius et al., 2003; Osinski et al., 2010), this makes the model operating in an eddy-resolving to eddy-permitting regime. The vertical resolution is 3 m in the upper layers, down to 60 m, and then gradually increases to 22 m at depths; the vertical discretization uses the z^* formulation and the bottom topography is represented by the partial steps approach. The setup utilizes a fully non-linear free surface formulation with a time splitting of barotropic and baroclinic modes to speed up simulation time. Vertical mixing is represented by the two equation generic length scale formulation (Umlauf and Burchard, 2005). In addition, Laplacian horizontal and isopycnal mixing is used in conjunction with a bottom-boundary layer parametrization (Beckmann and Döscher, 1997).

For further details and evaluation of the NEMO-Nordic ocean model setup the reader is referred to Hordoir et al. (2015).

2.1.2 The Sea Ice Model

LIM3 is a dynamic–thermodynamic sea-ice model with a multi-category ice thickness distribution and multi-layer halo-thermodynamics (Vancoppenolle et al., 2009; Rousset et al., 2015). The ice dynamics use a modified elastic-viscous-plastic (EVP) rheology (e.g. Bouillon et al., 2009) and accounts for sea-ice deformation processes (ridging and rafting).

The present NEMO-Nordic builds upon version 3.6 of LIM3. Compared to the polar oceans, sea ice[1] in the Baltic Sea is only seasonal, generally thinner, and with a much lower brine content due to the low salinities in the Baltic Sea. Thus, some model parameters need to be adjusted to the Baltic Sea conditions. In Table 1 we show the settings of the physical sea ice parameters that were adjusted in our NEMO-Nordic setup. The settings are also compared to that of a large-scale global ocean configuration ORCA2-LIM3, a configuration that is include in the NEMO–LIM3.6 model system. Below we briefly describe the rationale behind most of these settings.

In NEMO-Nordic the ice thickness distribution is discretized using 5 different categories and the thermodynamic calculations uses 2 vertical layers of ice and 1 layer of snow. When new ice forms in open water it is assumed to have a thickness of 0.01 m. In our setup we neglect all internal halodynamical processes of the sea ice and use a constant bulk salinity of 0.001 g kg^{-1}, which essentially means that the effect of brine pockets is neglected. This value is 10% of the river salinity used in the model and was chosen for numerical stability reasons. We tested an ice salinity of 0.0 g kg^{-1} but that yielded an unstable model, likewise with an ice salinity higher than the river water salinity. For numerical stability reasons ice models also require some horizontal diffusion. In our configuration, with a relatively high horizontal resolution, we use a relatively low diffusivity constant of 1.0 m^2 s^{-1}. LIM3 has a ridging scheme that accounts for the thickness growth due to sea-ice ridging. In this scheme there is a parameter rn_hstar that adjusts the upper bound of the ridged ice thickness. Since ridges are generally thinner in the Baltic Sea compared to polar oceans we lowered rn_hstar to 30.0 m from the default 100.0 m, likewise we lowered the crossover thickness for when sea ice ridged instead of raft to 0.07 m instead of the more common value 0.17 m.

In addition, we have implemented a simple fast ice parametrization since this is not included in the present version of LIM3. Fast ice is an important feature of the Baltic Sea ice cover and usually occurs in coastal and archipelago regions where the ocean depth is shallow. This is done by simply masking out grid points where the depth is below 15 m in the dynamical components of LIM3 so that the ice remains stationary. The fast ice mask is deactivated if the total ice volume in a cell is below 0.001 m^3, which means that for extremely low concentrations there can be advection of ice in the fast ice zone. The main effect of the fast ice parametrization is that a region of more or less undeformed ice is formed close to the coasts, and that the ridges are formed outside of this region.

2.2 Ice thickness distribution

On spatial scales of O(km), the scale of most sea-ice models, the ice thickness varies considerably due to both thermodynamical growth and mechanical redistribution of ice. To account for such sub-grid scale ice thickness variations sea ice is described in terms of an ice thickness distribution $g(h)$, following Thorndike et al. (1975). Here $g(h)dh$ gives the areal fraction of ice with a thickness between h and $h + dh$. From the distribution we can calculate the ice concentration A as

$$A(x,y,t) = \int_0^\infty g(h,x,y,t)\,dh, \tag{1}$$

---

[1]In fact, on a micro-scale it is brackish ice rather than sea ice. However, the brackish Baltic Sea ice can still be assumed to behave as sea ice (Leppäranta and Myrberg, 2009).

and the mean thickness as

$$H(x,y,t) = \int\limits_{0}^{\infty} h\, g(h,x,y,t)\, dh. \tag{2}$$

In LIM3 the ice thickness distribution is discretized by defining n ice categories with thickness bounds H_i^{lower} and H_i^{upper} for category i. Usually 5 categories are sufficient to resolve the sub-grid scale distribution (Bitz et al., 2001). Within each category the ice thickness is free to evolve between H_i^{lower} and H_i^{upper}, and as thermodynamical and dynamical processes form or melt the ice, the ice thickness changes and LIM3 accordingly remaps the ice thickness distribution to account for this.

For regional applications, where sea ice usually is thinner than in the polar regions, LIM3 has a new scheme to calculate the ice category bounds (Rousset et al., 2015). Based on an expected domain average ice thickness $\overline{h}$ the category bounds are fitted to a function $(1-h)^\alpha$ on the interval between 0 and $3\overline{h}$. In NEMO-Nordic the ice thickness distribution is discretized using 5 different categories based on a $\overline{h} = 0.5$ m giving the lower bounds: 0.0, 0.25, 0.56, 0.95 and 1.46 m (also shown in Fig 8a).

To compare the simulated thicknesses with observations we use two different metrics:

$$\overline{H} = \frac{\sum_{i=1}^{5} g_i h_i}{\sum_{i=1}^{5} g_i}, \tag{3}$$

which is the mean ice thickness for each grid cell, the discrete counter-part of Eq. 2 (also called cell-averaged thickness); and

$$\overline{H}_{level} = \frac{\sum_{i=1}^{4} g_i h_i}{\sum_{i=1}^{5} g_i}, \tag{4}$$

which is a proxy for the undeformed level ice. The upper bound for the fourth category is 1.46 m which is greater than the maximum thermodynamical ice growth for most conditions of the present Baltic Sea state. In addition, there is a distinct separation in the ice thickness distribution between the first four and the last category, see Fig. 8 (this is discussed more in section 3.3). We interpreted this as representing a separation between the thermodynamically and dynamically grown ice, and thus use the first four ice categories as a proxy for level ice and the fifth category as a proxy for ridged ice. We stress that this is just an approximation as rafting and smaller ridges will also be represented by the model in the lower categories. However, for many applications (e. g. maritime winter traffic) it is the actual thickness rather than the underlying processes that is important.

2.3 Forcing and simulation

As atmospheric forcing we use downscaled ERA-40 reanalysis data (Uppala et al., 2006) which, compared to the original ERA-40 reanalysis, features additional regional details which considerably affect the solution of standalone ocean models of the Baltic Sea (Meier et al., 2011). Note that the ERA-40 data set only covers the period up until 2002 and afterwards we use operational analysis from the ECMWF (European Centre for Medium-Range Weather Forecasts) for the downscaling. Using a different data set for the last 4 years could potential impact our results, however, our analysis show no evidence of that. The downscaling procedure takes ERA-40 reanalysis data as boundary conditions for the regional Rossby Centre Atmosphere model (hereafter RCA) which features an enhanced (relative to ERA-40) horizontal resolution of 25 km (Jones et al., 2004;

Samuelsson et al., 2010). As shown by Samuelsson et al. (2010) the approach provides a very realistic climatology. This downscaling approach was successfully used in earlier studies (e.g. Dietze et al. (2014), Hordoir and Meier (2011), Hordoir et al. (2013), Löptien and Meier (2011), Löptien et al. (2013)). The present forcing is an advancement as it uses the updated atmospheric model RCA4 and spectral nudging (Berg et al., 2013), which ensures that the simulated cyclone paths match the actual tracks.

5   This atmospheric forcing is applied to NEMO-Nordic in a 45-year long (1961–2006) hindcast simulation. The simulation is initialized from rest with climatological salinity and temperature distributions. The simulation starts in January 1961 with no ice present in the model. As the seasonal sea ice disappears every summer the spinup of the ice cover is usually short and already at the next winter the ice cover is well adapted. To account for the ice spinup we start our analysis in the beginning of the 1961/62 ice season. On the open boundary in Kattegat the model is forced by sea level variations from daily tide gauge

10   data. For temperature and salinity on the open boundary and runoff draining into the Baltic Sea we use monthly climatological values. Meier et al. (2012) showed that, for temperature such an approach is sufficient for the Baltic Sea as most of the trend comes from the atmospheric forcing. However, in Kattegat close to the open boundary in the sub-region, the solution can of course be affected by the simplified boundary conditions.

15   **2.4   Observational Data**

We use several observational data sets to evaluate the sea ice model. An extensive historical data set, named BASIS, covers the winters 1960/61 to 78/79. This data set contains the, at that time, best available information on the ice concentration, thickness as well as on the dominant ice types. BASIS is based on hand drawn sea ice charts which were provided by the local weather services for shipping. These ice charts were collected and then digitized 1981 in a joint project of the Finnish Institute of Marine

20   Research (today FMI) and SMHI. The original data were hard to access as BASIS-ice was designed for storage on punchcards. Thus, Löptien and Dietze (2014) provided an easier to access version in the free file format NetCDF via www.baltic-ocean.org (or PANGEA doi:10.1594/PANGAEA.832353).

In addition to BASIS, we use modern ice charts, called IceMaps, (which interpolate various observations on sea ice); the Swedish Ice Service of SMHI also provided weekly ice thickness measurements (1971–2010) in the fast ice zone at the stations

25   Järnäs (19.41E 63.26N) and Kemi (24.31E 65.4N). These are located in the Bothnian Bay and Bothnian Sea, respectively. Additionally, we use airborne EM-ice thickness measurements in the basin interiors of the Gulf of Finland and Bothnian Bay, which were collected 23th of February 2003, 14th of March 2004 and 13th of March 2005, all within the IRIS-project (Haas, 2004). It is, however, important to keep in mind that comparing point measurements to the model accounts for very different scales and has to be considered with some caution.

30   To evaluate the sea surface temperature (SST) we use CTD casts from SMHI and a satellite derived data set from the Bundesamt für Seeschifffahrt und Hydrographie (BSH). The CTD casts where done on a close to monthly basis at the stations Anholt E, Fladen, BY15 and BY31 (see Fig. 1) here we use data for the periods 1965–2006, 1971–2006, 1963–2006 and 1961–2006 respectively. The BSH data consist of high-quality satellite SST data product compiled into a monthly data set covering

the period 1990–2006. Also here it is important to be cautious when interpreting model biases as the modeled SST represent the temperature of the upper 3 m whereas the CTD cast and BSH represent the near-surface and surface values, respectively.

2.5 Freezing degree days model

To evaluate NEMO-Nordic in the coastal fast ice zone we compare the model to the ice thickness growth based on a simple
5   freezing degree days (FDD) model. In this kind of simple model the ice growth is purely thermodynamical and estimated from the cumulative number of days when the air temperature is below the freezing temperature. In its most simple form the FDD model assumes bare ice, i.e. no snow, and uses a linear air–ice heat flux. The FDD model can be formulated as (see e.g. Leppäranta and Myrberg, 2009)

$$h(\Theta) = (a^2\Theta + c^2)^n - c, \qquad\qquad\qquad (5)$$

10   where h is the ice thickness, Θ the number of FDD. Here we use, following Luomaranta et al. (2014), $a = 3.0$, $c = 10.0$ and $n = 0.5$. Θ is calculated as

$$\Theta = \int T_f - T\, dt, \qquad\qquad\qquad (6)$$

where T_f is the freezing temperature and T the daily mean temperature. Note that only days when $T < T_f$ in (6) is considered. This type of model only estimates the sea-ice thickness during the growth season until the maximum is reached and not the
15   melting season when sea ice starts to thin. Furthermore, as snow is omitted the thickness estimated from the FDD model represents an upper limit of the pure thermodynamical growth.

3   Model Evaluation

In this section we evaluate NEMO-Nordic's performance against a set of different observational data sets. The main focus is on the long-term statistics of important sea-ice parameters such as sea-ice concentration, extent and thickness. For the
20   climate system any changes in these sea-ice parameters are crucial and are thus important to evaluate for future climate studies and related studies on e.g. winter navigation and hazard. We also briefly compare single days when the ice cover reached its maximum extent, for 2 extreme winters. This is done to evaluate the model's capability to capture extremes on daily time scales which is important for forecasting purposes. However, we stress that the model data is from a hindcast simulation, which is a totally different mode of operation compared to how sea-ice forecasts are run. Before evaluating the sea-ice parameters we
25   evaluate the simulated the SST.

3.1   Sea surface temperature bias

The SSTs reflect the air-sea interaction of heat and biases in the SSTs indicate that either the atmospheric forcing and/or the ocean dynamics could be misrepresented. Any such biases will also affect the growth of sea ice and we therefore briefly evaluate the SST biases in NEMO-Nordic in the following. Here we compare the simulated SST with a satellite derived SST

product from BSH and with CTD casts at a few stations in the Baltic Sea and Kattegat. Figure 2 shows the long-term (1990–2006) wintertime SST biases over the model domain. We caution that in regions which usually are ice-covered these means are heavily weighted to ice-free conditions as the satellite sensor has limited capabilities to estimate under-ice SSTs. As seen in Fig. 2 NEMO-Nordic tends to be colder than the BSH data set over most of the model domain, for the January–March period.

5 An exception is in the Gulf of Riga where there is a persistent positive bias. Some parts of the central Baltic Proper and Gulf of Finland also exhibit a small positive bias. In April, on the other hand, NEMO-Nordic has a positive bias over much of the Baltic Proper. Another evident feature is that there is a persistent strong negative bias in Kattegat. These results are inline with the study by Gröger et al. (2015) who found that the dynamical downscaling of ERA-40 has a cold bias, due to a cold bias in the prescribed SST, particularly in Kattegat and the Baltic Sea, which in their forced simulation lead to too cold SSTs. The BSH

10 data only cover the last two decades of the simulation and to further evaluate the simulated SSTs we compared NEMO-Nordic with CTD data from four different stations which has long-term monitoring, two in the Baltic Sea (BY15 and BY31) and two in Kattegat (Fladen and Anholt E). Figure 3 compares January–April SSTs from NEMO-Nordic with the CTD data at the different stations. Here simulated daily averages where extracted from the same dates and periods as the individual stations. Also here it is evident that there is a systematic bias in Kattegat while in the Baltic Sea the observations and NEMO-Nordic

15 SSTs seem to better match. The long-term means for the Fladen, Anholt E, BY15 and BY31 are -0.7, -0.7, 0.2 and -0.1 °C, respectively. If we exclude all data prior to 1990 (not shown) the results are almost identical, with only BY15 and Fladen becoming roughly -0.1 colder in NEMO-Nordic. We note that the model suffers from a negative SST bias which is especially pronounced in Kattegat. Further, the CTD data confirm that the bias is persistent in Kattegat over the entire simulation. In the Baltic Sea, on the other, the two data sources disagree on the SST biases for the same period, the BSH data show a negative

20 bias at both stations while the CTD data show a lower smaller negative bias at BY31 and a small positive bias at BY31. We also note that the satellite derived data set yields a larger negative bias for all stations, compared to the CTD data, for the same periods. Whether the basin scale negative bias evident in the BSH data comparison is present in the first three decades can not be determined from these data sources. It is beyond the scope of the present study to further explore the underlying reasons behind the SST biases.

25 3.2 Sea-ice concentration and extent

The extent of the sea-ice cover and its concentration are two important parameters that a sea-ice model needs to simulate well both from a climatological and forecasting perspective. Here we show the long-term spatial coverages and the time variability of the total sea-ice extent in the Baltic Sea.

Figures 4 and 5 show the long-term (1961–1979) monthly mean sea-ice concentrations for both NEMO-Nordic and the

30 BASIS data set. As seen the general agreement is quite good for this period. In January both the model and BASIS agree on the coverage in the Bothnian Bay, Bothnian Sea, Gulf of Finland and Gulf of Riga. However, the ice coverage in Kattegat is much overestimated in NEMO-Nordic. In February when the Baltic Sea ice coverage usually reaches its maximum NEMO-Nordic and BASIS agrees very well showing that the Bothnian Bay and Sea, Gulf of Finland and Gulf of Riga are completely ice-covered. The Belt Sea and Kattegat are also completely ice-covered but with much lower ice concentration while only the

coastal regions in the Baltic Proper and Arkona Sea on average are ice-covered. In March the agreement is also good although NEMO-Nordic simulates some sea ice in Kattegat. In April the reduction of sea ice is evidently stronger in the model which shows much less ice in the Bothnian Sea and Gulf of Riga.

The annual maximum Baltic Sea ice extent (MBI) is a widely used metric to describe climate variability in the region, and the first recordings date back to 1720 (e.g. Vihma and Haapala, 2009, and reference therein). To evaluate the MBI we compare NEMO-Nordic with observational estimates from BASIS extended with IceMaps from the Swedish Ice Service. Note that in this study sea-ice extent is calculated as the area where sea-ice concentration is at least 15%; and that we have excluded sea ice in the Skagerrak region in the observational estimates as this region is missing in the present configuration. Figure 6 shows that the model captures the variability quite well. The simulated and observed standard deviations are 78 and 98 km^2, respectively, and the correlation between the model and observations is 0.85. However, the simulated trend (-10 km^2/decade) for the 1961–2006 period is much lower than the observed trend (-40 km^2/decade). For a level of $p \leq 0.05$ the null hypothesis of no trend could not be rejected for the simulated trend ($p = 0.27$); while the observed trend ($p = 0.0002$) falls well below this level. Excluding Kattegat in the trend analysis yield a much lower trend in the observational data set (-17 km^2/decade), while the simulated trend (-5 km^2/decade) is similar to the trend including Kattegat. This shows that the model has a persistent bias in the Kattegat region.

In the Baltic Sea ice winters are usually classified, following Seinä and Paluso (1996), as: mild, average, severe and extremely severe based on the MBI. For the period 1961–2006 NEMO-NORDIC (observational estimates) shows 8 (11) mild, 25 (16) average, 10 (13) severe and 2 (5) extremely severe winters. Clearly the classification statistics show that the model has a tendency to overestimate the number of average MBIs while the extreme cases are underestimated, which is related to the lower trend.

Figure 7 shows the long-term mean monthly seasonal cycles and standard deviations. Again NEMO-Nordic is well in line with the observational estimates, however, the reduction of sea ice during spring tends to occur earlier in the season in the model. This offset is especially pronounced during the first two decades (not shown).

Overall NEMO-Nordic agrees well with the BASIS data sets in terms of sea-ice concentration and extent. The offsets with a too high sea-ice extent in Kattegat and the overestimation of the total sea-ice extent the in last three decades are both inline with the already discussed SST biases.

3.3 Sea-ice thickness, volume and deformation

Sea-ice thickness is another important sea-ice parameter that both reflects the thermodynamical and dynamical evolution of the ice pack. Here we evaluate the sea-ice thickness distribution as well as the long-term mean sea-ice thickness, sea-ice volume and ice concentration in the thickest category, where the latter is used as a proxy for the sea-ice ridge concentration.

The sea-ice thickness distribution yields information of both the thermodynamical and dynamical ice growth. The dynamical ice growth tends to affect the extreme ends of the distribution when ridging and rafting creates thicker ice and open water while thermodynamical processes tend to populate the distributions towards a center value (Weeks, 2010). Figure 8 shows the simulated and observationally estimated sea-ice thickness distributions, calculated as an average of the three days during

2003–2005 winters when the EM-ice thickness measurements were carried out. As seen in Fig. 8b the sampling is quite sparse and mostly reflects the conditions in the central Bothnian Bay and Gulf of Finland, regions where we expect to find a wide range of thicknesses, including ridges. The mean thicknesses of NEMO-Nordic and the observational estimates are 84 and 113 cm, respectively. Compared to the observational estimates NEMO-Nordic has a more bi-modal distribution which

5 overestimates the thickness in the ranges $0.4 - 0.5$ m and $3.0 - 4.0$ m while sea-ice in the thickness range $1.2 - 2.8$ m is strongly underestimated. The observational data set is sampled on a finer spatial scale and is then averaged onto the NEMO-Nordic grid. This presumably affects the distribution. In addition, the rather coarse discretization with only five categories and the maximum ridge ice thickness limit in the ridging parametrization probably also impact the differences. We also note that the model used in Löptien et al. (2013) that utilizes adaptable ice category limits seems to better resolve the Baltic Sea ice

10 thickness distribution, particularly in the $1.2 - 2.8$ m range (c.f their Fig. 7a with our Fig. 8a). However, Fig. 8a also shows that there is a distinct separation between dynamically and thermodynamically grown ice in the model just below the lower limit (1.46 m) of the thickest ice category. This gives merit to using the four lowest ice categories as a proxy for level ice and the thickest ice category as a proxy for ridged ice. Hence we apply this concept as NEMO-Nordic does not have an explicit ice category for ridged ice.

15 We now compare the proxy level ice thickness, proxy ridged ice concentration and the area-integrated ice volumes in NEMO-Nordic with observational estimates from BASIS. The level ice thickness in the model is calculated as a category-weighted average of the first four ice categories, see Eq. 4. This metric mainly reflects the thermodynamical growth of the model. As seen in Figures 9 and 10 NEMO-Nordic and BASIS agree very well on both the absolute magnitude and the spatial gradients in the level ice thickness. Both show the transition towards gradually thicker ice in the northern Bothnian Bay and eastern Gulf

20 of Finland, there is also a gradient with thicker ice close to the coasts and thinner ice more central in the basins in both sources. The main difference is an overestimation by the model of the ice thickness in the fast ice zone, close to the Finnish west coast, for all compared months. From the long-term January–April level ice thickness means we then calculate the area-averaged level ice thickness for the Bothnian Bay, Bothnian Sea and Gulf of Finland which yield for NEMO-Nordic (BASIS): 37 (39), 14 (13) and 22 (23) cm, respectively.

25 Figure 11 compares the proxy ridge ice concentration from NEMO-Nordic with observational estimates from BASIS. Here the agreement is generally good between the model and the observational estimates, both show a high concentration in the central Bothnian Bay, and lower concentrations close to the coast in the Bothnian Sea and eastern part of Gulf of Finland, regions where we expected to find ridges. It is also seen how the fast ice parametrization leads to much lower deformed ice concentrations close to the coasts. However, we stress that these are two different measures of the ridging: the observations

30 estimate the number of ridges per kilometer while the model proxy gives the areal fraction of all ice thicker than 1.46 m in a model grid cell.

To further explore the composition of the different ice categories we calculate the area-integrated ice volume per ice category, integrated over the Bothnian Bay and the entire Baltic Sea, as an average of the January–April 1961–1979 period. From Fig. 12 we can see that a large portion (25–50%) of the ice volume is found in the thickest ice category, both for the Bothnian Bay and

35 the entire Baltic Sea, especially late in the ice season. Compared to the BASIS data set the total ice volume in NEMO-Nordic

is (18–36%) higher, particularly in the Bothnian Bay. For the entire Baltic Sea region the total sea-ice volume better matches the observational estimates, here the fraction of thin ice is also greater in the model. Additionally, Fig. 12 clearly shows the redistribution of ice towards thicker categories as the ice season evolves.

Figures 9–12 show that, compared to BASIS, NEMO-Nordic generally agrees well on the spatial patterns and area-averaged level ice thickness, but has a greater total ice volume. Observations of ridges are usually quite sparse and BASIS reflects the level ice thickness and volume. As the simulated volumes imply that the deformed ice constitutes a considerable amount of the total volume this primarily explains the differences in total ice volumes both for the Bothnian Bay and the total domain. Other factors that could impact the difference are biases in the snowfall rate, air temperature and/or wind forcing. As already discussed, Gröger et al. (2015) found that over the Baltic Sea region the air temperature and windstress in the dynamical downscaling of ERA-40 is generally lower and higher, respectively. This implies that these biases in the atmospheric forcing parameters would lead to an overestimation of the total ice volume. If we exclude the volume in the fifth category we have an estimate of the simulated level ice volume which, on the other hand, is lower than the observed total volume. Thus, the mean ice thickness from the thickness distribution, the long-term January–April area-averaged level ice thickness and the area-integrated level ice volume all show that NEMO-Nordic has a lower ice thickness/volume compared to BASIS and EM measurements.

3.4 Coastal stations in fast ice zone

The sea ice in the coastal regions around the Baltic Sea usually consist of (land) fast ice which is immobile. These areas are important platforms for both human activity and marine wild life. Here the ice pack is dominated by thermodynamical growth driven by the changes in surface air temperature. In the initial stages the wind conditions also affect the formation and extent of the fast ice. The fast ice zone also affects the atmosphere–ocean momentum interaction as the wind stress is damped out. To evaluate the model performance we first compare simulated cell-averaged ice thickness with long-term weekly ice thickness observations at two coastal stations, outside Ratan and Järnäs (see Fig. 1 for the locations). Then we proceed with comparing simulated cell-averaged ice thickness outside Luleå and Kemi with ice growth estimates based on a FDD model.

Figure 13 shows the long-term mean and standard deviations of simulated and observed sea-ice thickness on the edge of the model's fast ice zone at the Ratan and Järnäs sites. At the Ratan site NEMO-Nordic simulates a too thin mean ice cover during the growth phase of the ice season, up until the observed melt starts, implying a too slow thermodynamical growth rate. The variability for the growth phase, on the other hand, matches the observations quite well. During the observed melt phase, the simulated ice cover generally still continues to increase for 1–3 weeks more, leading to a shift in the mean seasonal cycle. The variability in this phase is much larger in the model, however, but the mean slope of melt matches the observations fairly well. At the Järnäs site the initial growth phase matches the observations better, with a similar growth rate and variability. The melt rate is also in line with the observation, however, there is still a shift in the mean seasonal cycle with the melt phase occurring a few weeks later in the season.

To further evaluate the ice growth in the fast ice zone we compare the simulated ice thickness outside Luleå and Kemi — two important ports in the Bothnian Bay – with a FDD ice growth model (see Eq. 5). Here we use the air temperature from the downscaled ERA-40 at the coastal sites to calculate ice thickness estimates for the 1962–2005 period. We chose the same

forcing as in the hindcast simulation to eliminate any uncertainties related to the forcing, selecting nearby air temperature observations would presumably yield more realistic results. As seen in Fig. 14 NEMO-Nordic agrees very well with both the mean thickness and variability during the growth season outside Luleå and Kemi. This means that NEMO-Nordic's ice growth at these locations is dominated by the thermodynamical growth. The slightly later onset of ice formation is presumably due to

5 ocean dynamics which can transport heat from nearby regions and maintain the sea surface temperatures above freezing for a few days to weeks longer than estimated by the FDD model. It is somewhat surprising to find that NEMO-Nordic matches the FDD model so well as NEMO-Nordic includes a snow cover that, at the Kemi location, varies with an annual maximum between 17–31 cm, for the investigated period. To further evaluate the simulated snow cover, the monthly mean snow cover at Kemi, calculated for the period 1979–1990 (see Fig. 15), was compared to the results reported by Saloranta (2000). Compared

10 to Saloranta's results (see his Fig. 4) our simulated annual maximum mean snow cover (24 cm) is in line with the observed snow cover (∼25 cm). For Kemi, Luomaranta et al. (2014) report an observed maximum ice thickness of 75 cm for the period 1971–2000. NEMO-Nordic compares well with this having a long-term maximum of 79 cm for the same period, our FDD model estimate yields 80 cm. Luomaranta et al. (2014) also estimate the growth using a FDD model but using air temperature from the E-OBS gridded dataset (Haylock et al., 2008). Here they find a somewhat higher maximum ice thickness of 98 cm,

15 for the same period, which they attribute to the lack of snow cover in their FDD model.

Here we used the cell-averaged thickness in the comparison with observations and a FDD model. Using the proxy level ice thickness (not shown) yields a slight underestimation at the Luleå, Kemi and Ratan sites and a larger underestimation at the more southern Järnäs site. For the latter two, which are just within the fast ice mask, it is evident that there is a signal of ridged ice late in the season affecting the seasonal cycles. Just as the ice breaks up and starts melting, small concentrations

20 of relatively thick ice are usually advected into the fast ice zone, and thus strongly influence the variability. Our results also demonstrate that it is not straightforward to compare simulated grid point values with point measurements, mainly due to the difference in scales. The observations represent the ice thickness for one point in space, while the cell-averaged ice thickness in a model grid cell represents the mean of the thickness distribution on the scale of ∼4 km. Another contributing factor to the difference in the seasonal cycles is that the measurements rely on a stable ice cover. When the ice starts to form or break up

25 it is much harder to go out and measure the thickness of the ice, thus the observations at the coastal stations Ratan and Järnäs underestimate the length of ice season.

3.5 Daily sea-ice extent and thickness for two extreme winters

To evaluate the model performance on shorter time scales we now briefly compare two single days from the hindcast with observational data from IceMap. We chose the day of the MBI for a mild winter (1995), and an extremely severe winter

30 (1987), see e.g. Fig. 6. In Fig. 16 we show the extent and level ice thickness for NEMO-Nordic and IceMap, where we chose the date of MBI in the IceMap data set for both sources. As seen in Fig. 16 the extent of NEMO-Nordic's ice cover agrees well with the IceMap ice cover. For the mild winter the MBI from IceMap was $64 \cdot 10^3$ km^2 and occurred on the 16th of February. For NEMO-Nordic the total ice extent for the same date was $69 \cdot 10^3$ km^2, but the seasonal maximum was somewhat larger ($95 \cdot 10^3$ km^2) and reached already five days earlier. For the extremely severe winter the MBI from IceMap was $369 \cdot 10^3$ km^2

and reached on the 5th of March. Here the NEMO-Nordic total ice extent was $353 \cdot 10^3$ km^2, while the maximum simulated extent of $377 \cdot 10^3$ km^2 was reached nine days later. We note that there is an offset for NEMO-Nordic both in the total size of the sea-ice extent and the time when it occurs for these two cases. The IceMap data is updated roughly two times per week, which could partly explain the offset. When the model is run in forecast mode data assimilation of SST and sea-ice concentration will

5 also likely improve the performance of the model, in terms of timing of the MBI furthermore.

For the mild winter the level ice thickness in NEMO-Nordic and IceMap agree quite well with the thickest ice found in the northern parts of Bothnian Bay, the eastern part of the Northern Quark and the eastern part of Gulf of Finland, while thinner ice is present in the central parts of the Bothnian Bay and along the coast of the Bothnian Sea. The area-averaged simulated ice thickness is somewhat thinner than the IceMap data. For the Bothnian Bay, Bothnian Sea and Gulf of Finland the NEMO-

10 Nordic (IceMap) area-averaged thicknesses are: 26 (29), 10 (14) and 21 (23) cm. For the extremely severe winter, on the other hand, only the broad scale features are similar between the two. NEMO-Nordic generally has thicker ice compared to IceMap except for in the northern parts of Bothnian Bay. The area-averaged NEMO-Nordic (IceMap) ice thicknesses for the Bothnian Bay, Bothnian Sea and Gulf of Finland are: 59 (54), 50 (31) and 53 (50) cm. It is also evident in Fig. 16 that the IceMap thickness data is very patchy and only represent the large-scale features of the ice pack.

15 **4   Summary and conclusions**

We have presented the ice component of a new NEMO–LIM3.6 based configuration of the Baltic Sea. The model system is intended to be used for both climate studies and short-term forecasting in the Baltic Sea region. To adapt NEMO-Nordic to the Baltic Sea a number of parameterizations were tuned to the brackish Baltic Sea conditions. Compared to, for instance, polar regions this means that we had to tune the model to the Baltic sea ice which is only seasonal, thinner and has a much lower

20 brine content. In addition, we implemented a simple fast ice parametrization which is based on the ocean depth.

In the present study we evaluated the performance of the model by comparing results from a 45-year long hindcast simulation, forced by data from a downscaled ERA-40 simulation, with several observational data sets. Most of our metrics are based on long-term changes in standard sea-ice parameters. However, we also briefly show how the model performs on a daily time scale by comparing daily means of the sea-ice state during the day of maximum extent for an extremely severe and mild winter.

25 Our results show that the sea-ice concentration and extent are generally very well simulated, when compared to the BASIS data set over the 1961–1979, although there is a bias in Kattegat, which might be related to a cold temperature bias in the air temperature forcing and the proximity to the open boundary. The downward trend of the MBI, over the 1961–2006 period, is much lower in NEMO-Nordic compared to the observational estimate. This is partly related to the general overestimation of the ice cover in the Kattegat region, which is also evident in the estimated SST biases.

30 The sea-ice thickness overall also agrees well with the observational data set. For the investigated period (1961–1979) the large-scale pattern shows good agreement between our level ice thickness estimate and the observations. The area-averaged thicknesses, area-integrated volumes of level ice, the mean ice thickness calculated from the ice thickness distribution, and the ice thickness at two selected stations along the Swedish coast all show that the model has a tendency to underestimate the level

ice thickness relative to the observational data sets. This is somewhat contradictory to what the negative SST biases imply. Here we speculate that a too thick snow cover could be a contributing factor. Our limited snow cover analysis show that at the Kemi site the snow cover seems to be inline with the reported observations by Saloranta (2000), however, this only represents one model point and further investigations of large-scale snow cover biases are needed to rule out a too thick snow cover as a cause

5 for the slight underestimation of the ice thickness. The ridged ice concentration is also generally in line with the observations, and the fast ice parametrization yields a more realistic distribution of the ridges. We caution that the observations, which are digitized hand drawn ice charts based on ship observations and various other sources, should be interpreted with some caution, as it is difficult to accurately estimate the ice thickness and deformation using that methodology. For future evaluations more objective methods should be preferred.

10 For the demonstrated extremely severe and mild cases of day of MBI, the total extent and spatial distributions are well in line with the observational estimate, although there is an offset in total extent and when the day occurs in the model. Here the estimated level ice thickness is generally overestimated by the model for the extremely severe case while the mild case agrees better with the observational data. However, the observations which are weekly ice charts are very patchy and only represent the large-scale features of the ice. In addition, data assimilation of SST and sea-ice concentration will presumably improve the

15 model skill further.

Furthermore, based on data from a few recent years the simulated ice thickness distribution shows a more bimodal distribution compared to the observational data set. Here better fine tuning of the ice category bounds, ridging parameters and more ice categories could possibly improve our model. However, we find that with the present ice category configurations the thickest ice category can be used as a proxy for ridge ice concentration and the lower four as proxy for level ice thickness and coverage.

20 Finally, we have implemented a very simple fast ice parametrization, which is fixed based only on the ocean depth. For climate studies and forecasting purposes a more sophisticated parametrization is needed to capture long-term and seasonal changes in the fast ice zone. Modeling of the fast ice zone has received relatively little attention but recent studies (Lemieux et al., 2015; Olason, 2016) have suggested new ways to parametrize the fast ice zone, which could be feasible for a Baltic Sea ice model.

25 5   Code and data availability

NEMO-Nordic builds on the standard NEMO code (nemo_v3_6_STABLE, revision 5628) with only minor changes including: the fast ice parametrization, a spatial varying background viscosity that could be read in from file and changes that allow for a simulation start time other than midnight. The standard NEMO code can be downloaded from the NEMO web site (http://www.nemo-ocean.eu/). The nemo_v3_6_STABLE version is available from the following link: http://forge.ipsl.jussieu.

30 fr/nemo/svn/branches/2015/nemo_v3_6_STABLE. Our Baltic Sea adopted code, input data, analysis scripts and data used to produce the figures in this study can be made available upon request by the corresponding author.

Acknowledgements. This research is part of the project BONUS STORMWINDS with financial support from BONUS, the joint Baltic Sea research and development programme (Art 185), funded jointly from the European Unions Seventh Programme for research, technological development and demonstration and from the Swedish research council for environment, agriculture sciences and spatial planning (FOR-MAS). This work is also partly funded by the SmartSea project of the Strategic Research Council of Academy of Finland, grant No: 292

5   985. We thank the Ice Service at SMHI as well as Christian Haas for providing data.

References

Alenius, P., Nekrasov, A., and Myrberg, K.: Variability of the baroclinic Rossby radius in the Gulf of Finland, Continental Shelf Research, 23, 563–573, doi:10.1016/S0278-4343(03)00004-9, 2003.

Beckmann, A. and Döscher, R.: A Method for Improved Representation of Dense Water Spreading over Topography in Geopotential-Coordinate Models, Journal of Physical Oceanography, 27, 581–591, doi:10.1175/1520-0485(1997)027<0581:AMFIRO>2.0.CO;2, 1997.

Berg, P., Döscher, R., and Koenigk, T.: Impacts of using spectral nudging on regional climate model RCA4 simulations of the Arctic, Geoscientific Model Development, 6, 849–859, doi:10.5194/gmd-6-849-2013, 2013.

Bitz, C. M., Holland, M. M., Weaver, A. J., and Eby, M.: Simulating the ice-thickness distribution in a coupled climate model, Journal of Geophysical Research: Oceans (1978–2012), 106, 2441–2463, doi:10.1029/1999JC000113, 2001.

Bouillon, S., Maqueda, M. A. M., Legat, V., and Fichefet, T.: An elastic–viscous–plastic sea ice model formulated on Arakawa B and C grids, Ocean Modelling, 27, 174–184, doi:10.1016/j.ocemod.2009.01.004, 2009.

Dietze, H., Löptien, U., and Getzlaff, K.: MOMBA 1.1 – a high-resolution Baltic Sea configuration of GFDL's Modular Ocean Model, Geoscientific Model Development, 7, 1713–1731, doi:10.5194/gmd-7-1713-2014, 2014.

Eilola, K., Mårtensson, S., and Meier, H. E. M.: Modeling the impact of reduced sea ice cover in future climate on the Baltic Sea biogeo-chemistry, Geophysical Research Letters, 40, 149–154, doi:10.1029/2012GL054375, 2013.

Funkquist, L. and Eckhard Kleine, E.: HIROMB An introduction to HIROMB, an operational baroclinic model for the Baltic Sea, Report Oceanography No 37, SMHI, [Available at http://www.smhi.se/publikationer], 2007.

Goerlandt, F., Montewka, J., Zhang, W., and Kujala, P.: An analysis of ship escort and convoy operations in ice conditions, Safety Science, pp. 1–12, doi:10.1016/j.ssci.2016.01.004, 2016.

Gröger, M., Dieterich, C., Meier, H. E. M., and Schimanke, S.: Thermal air–sea coupling in hindcast simulations for the North Sea and Baltic Sea on the NW European shelf, Tellus A, 67, doi:10.1029/2004JC002378, 2015.

Haapala, J., Markus Meier, H. E., and Rinne, J.: Numerical Investigations of Future Ice Conditions in the Baltic Sea, AMBIO: A Journal of the Human Environment, 30, 237–244, doi:10.1579/0044-7447-30.4.237, 2001.

Haas, C.: Airborne EM sea-ice thickness profiling over brackish Baltic sea water, in: 17th International Symposium on Ice, pp. 1–17, Saint Petersburg, Russia, 2004.

Haylock, M. R., Hofstra, N., Klein Tank, A. M. G., Klok, E. J., Jones, P. D., and New, M.: A European daily high-resolution gridded data set of surface temperature and precipitation for 1950–2006, Journal of Geophysical Research, 113, D20 119, doi:10.1029/2008JD010201, 2008.

HELCOM: Recommendation 25/7 on Safety of winter navigation in the Baltic Sea Area, Baltic Marine Environment Protection Commission (Helsinki Commission), available at http://www.helcom.fi/, 2004.

HELCOM: Ensuring safe shipping in the Baltic, Baltic Marine Environment Protection Commission (Helsinki Commission), available at http://www.helcom.fi/, 2009.

Hordoir, R. and Meier, H. E. M.: Effect of climate change on the thermal stratification of the baltic sea: a sensitivity experiment, Climate Dynamics, doi:10.1007/s00382-011-1036-y, 2011.

Hordoir, R., Dieterich, C., Basu, C., Dietze, H., and Meier, H. E. M.: Freshwater outflow of the Baltic Sea and transport in the Norwegian current: A statistical correlation analysis based on a numerical experiment, Continental Shelf Research, 64, 1–9, doi:10.1016/j.csr.2013.05.006, 2013.

Hordoir, R., Axell, L., Löptien, U., Dietze, H., and Kuznetsov, I.: Influence of sea level rise on the dynamics of salt inflows in the Baltic Sea, Journal of Geophysical Research, pp. n/a–n/a, doi:10.1002/2014JC010642, 2015.

Jones, C. G., Willén, U., Ullerstig, A., and Hansson, U.: The Rossby Centre Regional Atmospheric Climate Model Part I: Model Climatology and Performance for the Present Climate over Europe, AMBIO: A Journal of the Human Environment, 33, 199–210, doi:10.1579/0044-7447-33.4.199, 2004.

Lemieux, J.-F., Tremblay, L. B., Dupont, F., Plante, M., Smith, G. C., and Dumont, D.: A basal stress parameterization for modeling landfast ice, Journal of Geophysical Research, 120, 3157–3173, doi:10.1002/2014JC010678, 2015.

Leppäranta, M. and Hakala, R.: The structure and strength of first-year ice ridges in the Baltic Sea, Cold Regions Science and Technology, 20, 295–311, doi:10.1016/0165-232X(92)90036-T, 1992.

Leppäranta, M. and Myrberg, K.: Physical oceanography of the Baltic Sea, Springer Science and Business Media, 2009.

Löptien, U. and Dietze, H.: Sea ice in the Baltic Sea–revisiting BASIS ice, a historical data set covering the period 1960/1961–1978/1979, Earth System Science Data, doi:10.1594/PANGAEA.832353, 2014.

Löptien, U. and Meier, H. E. M.: The influence of increasing water turbidity on the sea surface temperature in the Baltic Sea: A model sensitivity study , Journal of Marine Systems, 88, 323–331, doi:10.1016/j.jmarsys.2011.06.001, 2011.

Löptien, U., Mårtensson, S., Meier, H. E. M., and Höglund, A.: Long-term characteristics of simulated ice deformation in the Baltic Sea (1962-2007), Journal of Geophysical Research, 118, 801–815, doi:10.1002/jgrc.20089, 2013.

Luomaranta, A., Ruosteenoja, K., Jylhä, K., Gregow, H., Haapala, J., and Laaksonen, A.: Multimodel estimates of the changes in the Baltic Sea ice cover during the present century, Tellus A, 66, 93, doi:10.3354/cr025217, 2014.

Madec, G.: NEMO ocean engine, Note du Pole de modélisation No 27, Institut Pierre-Simon Laplace (IPSL), [Available at www.nemo-ocean.eu], 2016.

Meier, H. E. M.: Baltic Sea climate in the late twenty-first century: a dynamical downscaling approach using two global models and two emission scenarios, Climate Dynamics, 27, 39–68, doi:10.1007/s00382-006-0124-x, 2006.

Meier, H. E. M., Döscher, R., and Faxen, T.: A multiprocessor coupled ice-ocean model for the Baltic Sea: Application to salt inflow, Journal of Geophysical Research, 108, 3273, doi:10.1029/2000JC000521, 2003.

Meier, H. E. M., Döscher, R., and Halkka, A.: Simulated distributions of Baltic Sea-ice in warming climate and consequences for the winter habitat of the Baltic ringed seal, AMBIO, 33, 2004.

Meier, H. E. M., Höglund, A., Döscher, R., Andersson, H., Löptien, U., and Kjellström, E.: Quality assessment of atmospheric surface fields over the Baltic Sea from an ensemble of regional climate model simulations with respect to ocean dynamics*, Oceanologia, 53, 193–227, doi:10.5697/oc.53-1-TI.193, 2011.

Meier, H. E. M., Hordoir, R., Andersson, H. C., Dieterich, C., Eilola, K., Gustafsson, B. G., Höglund, A., and Schimanke, S.: Modeling the combined impact of changing climate and changing nutrient loads on the Baltic Sea environment in an ensemble of transient simulations for 1961–2099, Climate Dynamics, 39, 2421–2441, doi:10.1007/s00382-012-1339-7, 2012.

Montewka, J., Goerlandt, F., Kujala, P., and Lensu, M.: Towards probabilistic models for the prediction of a ship performance in dynamic ice, Cold Regions Science and Technology, 112, 14–28, doi:10.1016/j.coldregions.2014.12.009, 2015.

Olason, E.: A dynamical model of Kara Sea land-fast ice, Journal of Geophysical Research, 121, 3141–3158, doi:10.1002/2016JC011638, 2016.

Osinski, R., Rak, D., Walczowski, W., and Piechura, J.: Baroclinic Rossby radius of deformation in the southern Baltic Sea, Oceanologia, 52, 417–429, 2010.

Rousset, C., Vancoppenolle, M., Madec, G., Fichefet, T., Flavoni, S., Barthélemy, A., Benshila, R., Chanut, J., Levy, C., Masson, S., and Vivier, F.: The Louvain-La-Neuve sea ice model LIM3.6: global and regional capabilities, Geoscientific Model Development, 8, 2991–3005, doi:10.5194/gmd-8-2991-2015, 2015.

Saloranta, T. M.: Modeling the evolution of snow, snow ice and ice in the Baltic Sea, Tellus A, 52, doi:10.3402/tellusa.v52i1.12255, 2000.

Samuelsson, P., Jones, C. G., Willén, U., Ullerstig, A., Gollvik, S., Hansson, U., Jansson, C., Kjellström, E., Nikulin, G., and Wyser, K.: The Rossby Centre Regional Climate model RCA3: model description and performance, Tellus A, 63, 4–23, doi:10.1111/j.1600-0870.2010.00478.x, 2010.

Seinä, A. and Paluso, E.: The classification of the maximum annual extent of ice cover in the Baltic Sea 1720–1995., Report series of the Finnish Institute of Marine Research No 20, Finnish Institute of Marine Research, 1996.

Thorndike, A. S., Rothrock, D. A., Maykut, G. A., and Colony, R.: The thickness distribution of sea ice, Journal of Geophysical Research, 80, 4501–4513, doi:10.1029/JC080i033p04501, 1975.

Umlauf, L. and Burchard, H.: Second-order turbulence closure models for geophysical boundary layers. A review of recent work, Continental Shelf Research, 25, 795–827, doi:10.1016/j.csr.2004.08.004, 2005.

Uppala, S. M., Kållberg, P. W., Simmons, A. J., Andrae, U., Bechtold, V. D. C., Fiorino, M., Gibson, J. K., Haseler, J., Hernandez, A., Kelly, G. A., Li, X., Onogi, K., Saarinen, S., Sokka, N., Allan, R. P., Andersson, E., Arpe, K., Balmaseda, M. A., Beljaars, A. C. M., Berg, L. V. D., Bidlot, J., Bormann, N., Caires, S., Chevallier, F., Dethof, A., Dragosavac, M., Fisher, M., Fuentes, M., Hagemann, S., Hólm, E., Hoskins, B. J., Isaksen, L., Janssen, P. A. E. M., Jenne, R., Mcnally, A. P., Mahfouf, J. F., Morcrette, J. J., Rayner, N. A., Saunders, R. W., Simon, P., Sterl, A., Trenberth, K. E., Untch, A., Vasiljevic, D., Viterbo, P., and Woollen, J.: The ERA-40 re-analysis, Quarterly Journal of the Royal Meteorological Society, 131, 2961–3012, doi:10.1256/qj.04.176, 2006.

Valdez Banda, O., Goerlandt, F., Montewka, J., and Kujala, P.: A risk analysis of winter navigation in Finnish sea areas, Accident Analysis and Prevention, 79, 100–116, 2015.

Vancoppenolle, M., Fichefet, T., Goosse, H., Bouillon, S., Madec, G., and Maqueda, M. A. M.: Simulating the mass balance and salinity of Arctic and Antarctic sea ice. 1. Model description and validation, Ocean Modelling, 27, 33–53, doi:10.1016/j.ocemod.2008.10.005, 2009.

Vihma, T. and Haapala, J.: Geophysics of sea ice in the Baltic Sea: A review, Progress in Oceanography, 80, 129–148, doi:10.1016/j.pocean.2009.02.002, 2009.

Weeks, W. F.: On sea ice, Universiy of Alaska Press, 2010.
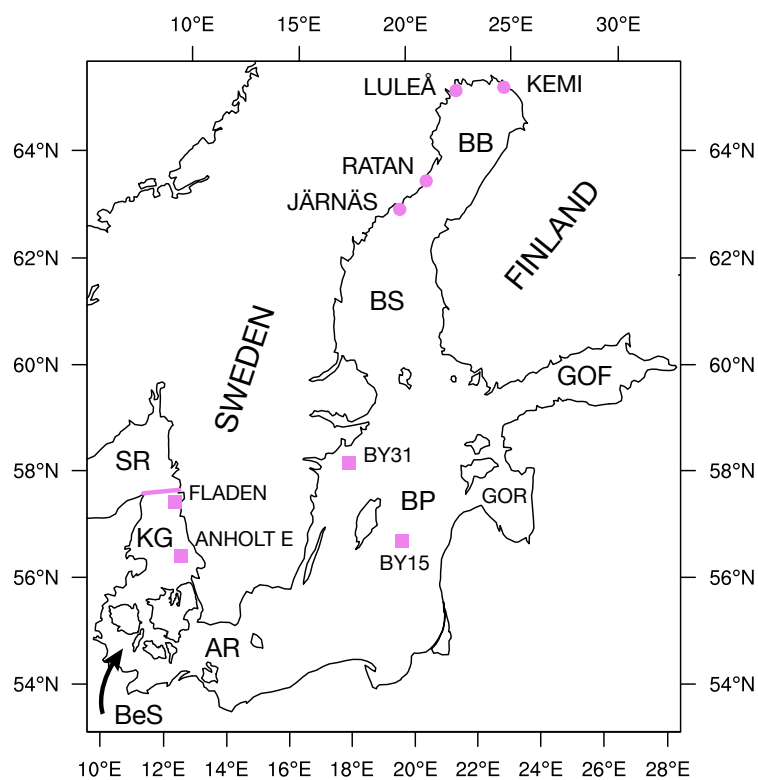
Figure 1. Map showing names of places mentioned in the text; the sub-basins are abbreviated: BB=Bothnian Bay, BS=Bothnian Sea, GOF=Gulf of Finland, GOR=Gulf of Riga, BP=Baltic proper, GR=Gulf of Riga, KG=Kattegat, AR=Arkona Sea, BeS=Belt Sea and SR=Skagerrak. The pink line shows the open boundary in Kattegat; the pink dots show the coastal sites Kemi, Luleå, Ratan and Järnäs; and the pink squares show the Fladen, Anholt E, BY15 and BY31 stations.
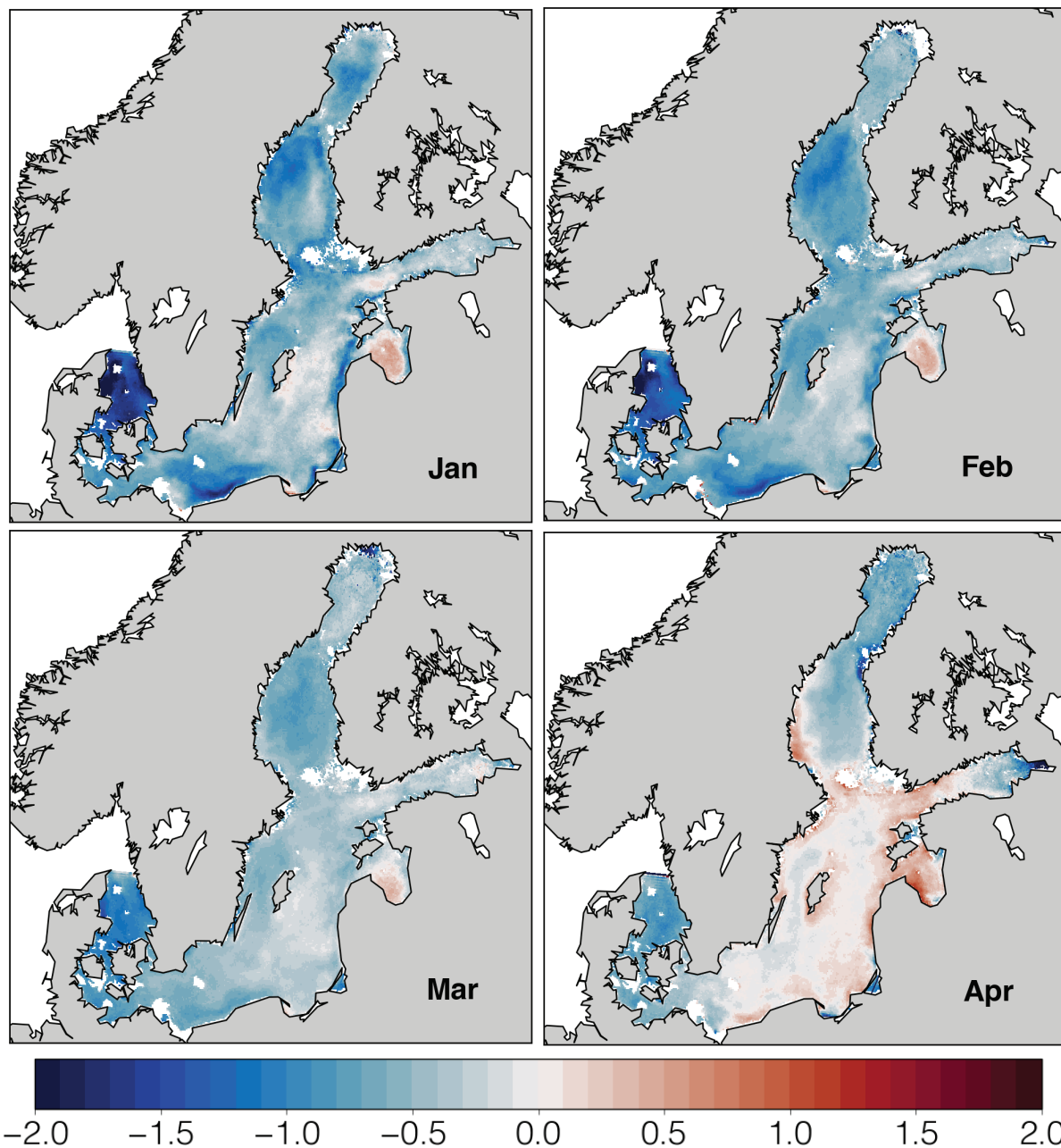
Figure 2. Long-term monthly mean January–April SST bias ($^{\circ}C$) for the period 1990/91–2005/06. Positive values means that NEMO-Nordic is warmer than the BSH satellite observations.
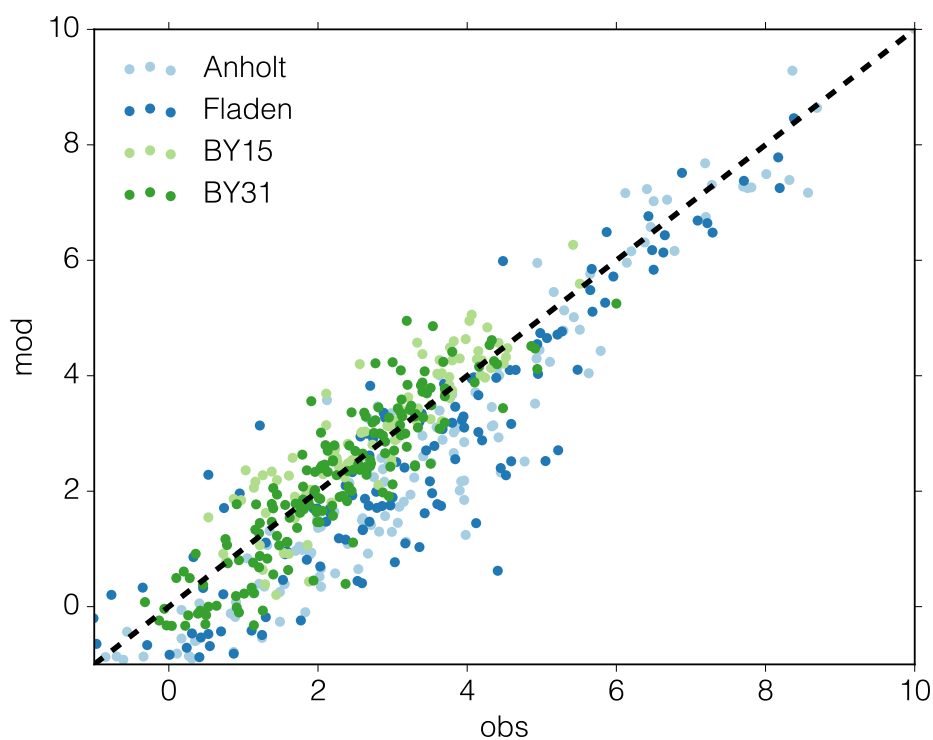
Figure 3. January–April SST bias for two stations in Kattegat (Fladen and Anholt E, blue colors) and two stations in the Baltic Sea (BY15 and BY31, green colors). SSTs estimated from CTD casts are on the x-axis and NEMO-Nordic SSTs on the y-axis; for the location of the different stations see Fig. 1.
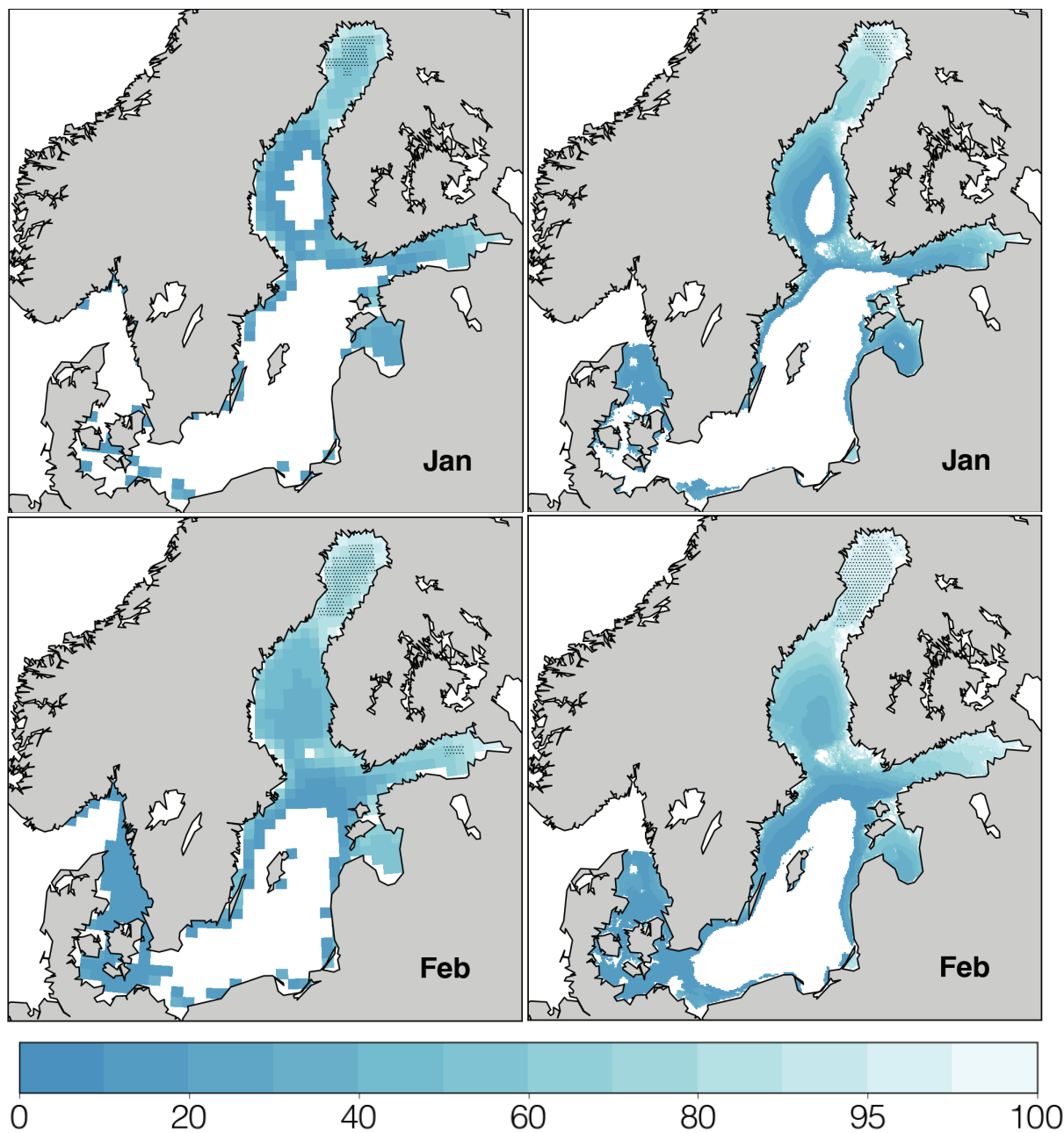
Figure 4. Climatological mean ice concentration for January and February, for the period 1961/62–1978/79. The left column shows sea-ice concentration for BASIS and the right for NEMO-Nordic. The hatched areas mark regions with more than 5% ridges (more than 5% of ice in the fifth ice category) for BASIS (NEMO-Nordic). Note that grid cells with an ice concentration lower than 15% have been masked out and that white areas denote missing or masked values.
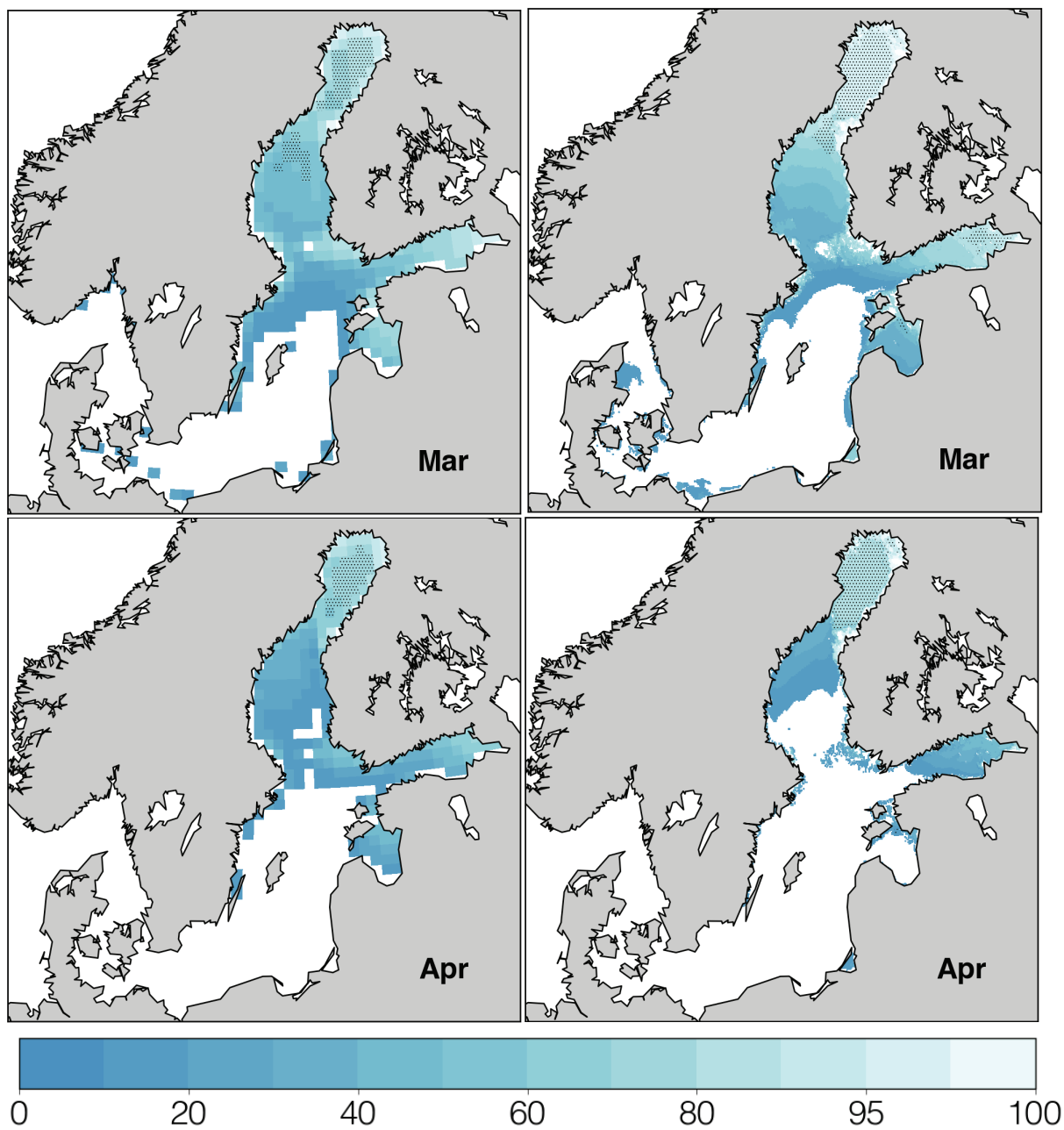
Figure 5. Same as Figure 4 but for March and April.
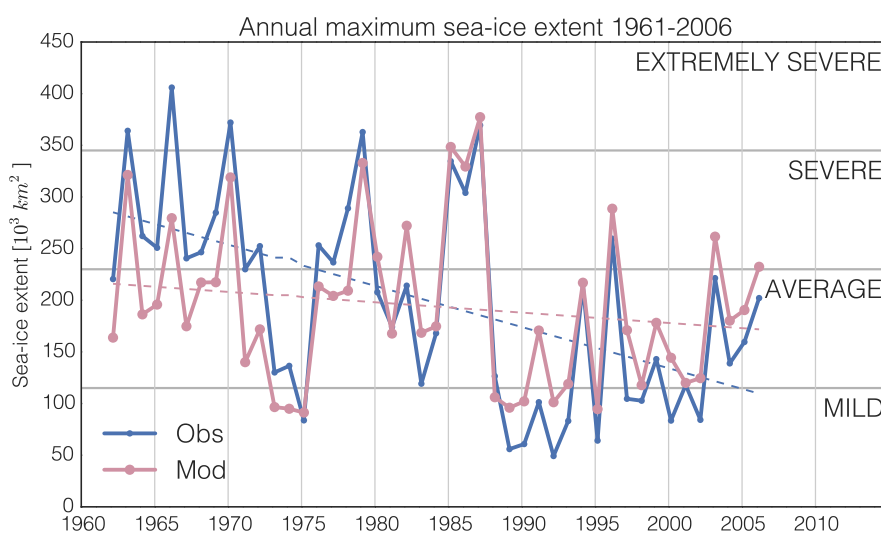
Figure 6. Simulated (red solid line) and observed (blue solid line) annual maximum daily sea-ice extent in the Baltic Sea, for the period 1961/62–2005/06. The horizontal gray lines show the limits for winters with a maximum sea-ice extent in the Baltic Sea classified as mild, average, severe and extremely severe, respectively. The dashed red and blue lines show the linear trends for simulated and observed maximum sea-ice extent, respectively.
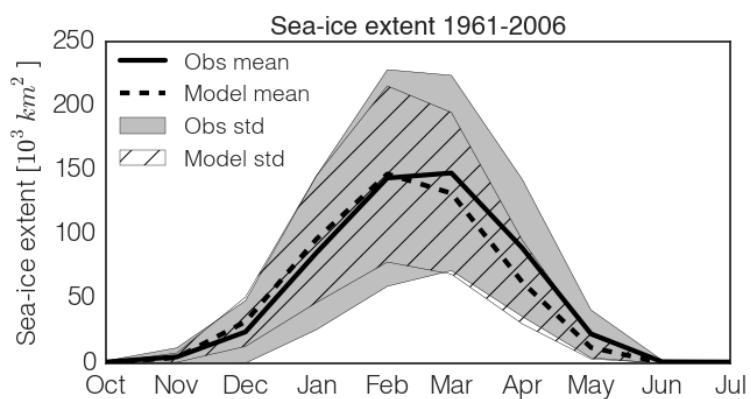
Figure 7. Seasonal cycles of simulated and observed total sea-ice extent in the Baltic Sea. The lines show the seasonal monthly means and the filled envelopes show the ± 1 standard deviations. The seasonal cycles are calculated for the periods 1961/62–2005/06. Note that Skagerrak has been masked out in the observational data set.
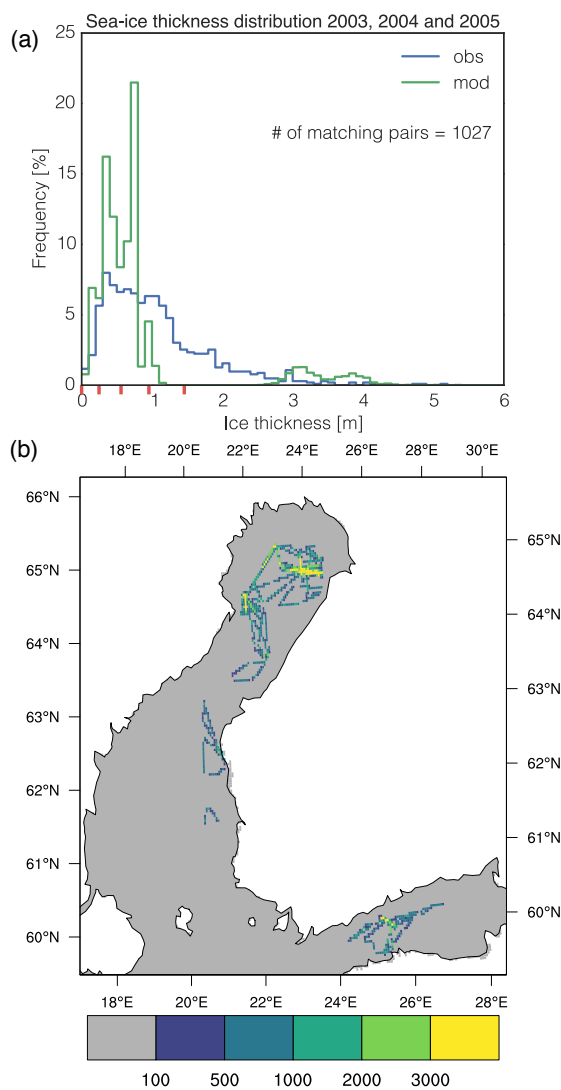
Figure 8. (a) Sea-ice thickness distributions calculated from the gridded EM data (blue) and the simulation (green). (b) shows the number of sub-grid observations of the gridded EM data. The red tick lines in (a) show the limits for the five ice categories, note that the upper limit of the last ice category – which is unbounded – is not shown.
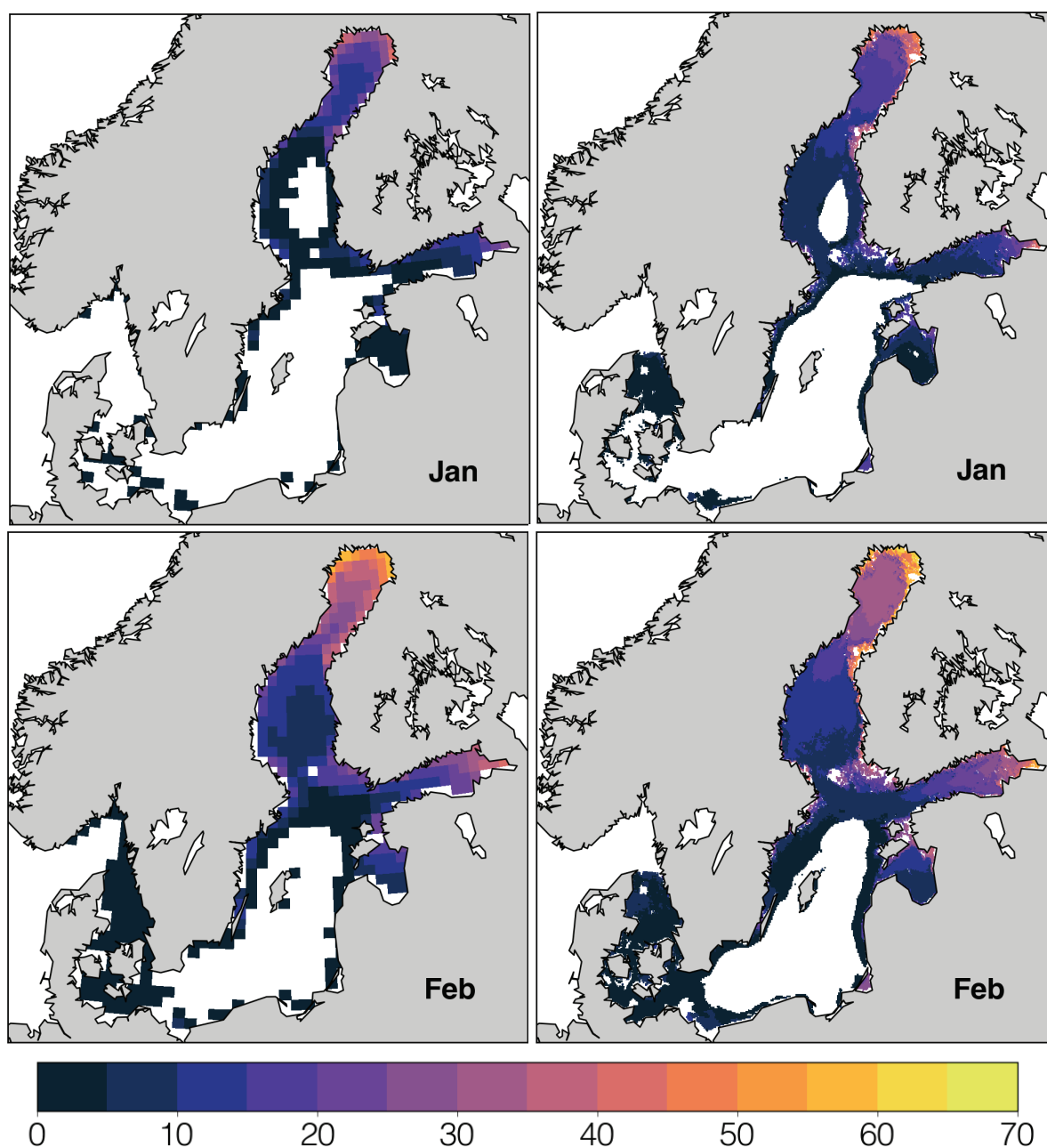
Figure 9. Climatological mean sea-ice thickness in cm for January and February, for the period 1961/62–1978/79. The left (right) column shows sea-ice thickness for BASIS (NEMO-Nordic). For NEMO-Nordic the mean sea-ice thickness represents a proxy level ice thickness and is calculated using a category-weighted average of the first four ice categories, see Eq. 4. Note that grid cells with an ice concentration lower than 15% have been masked out.
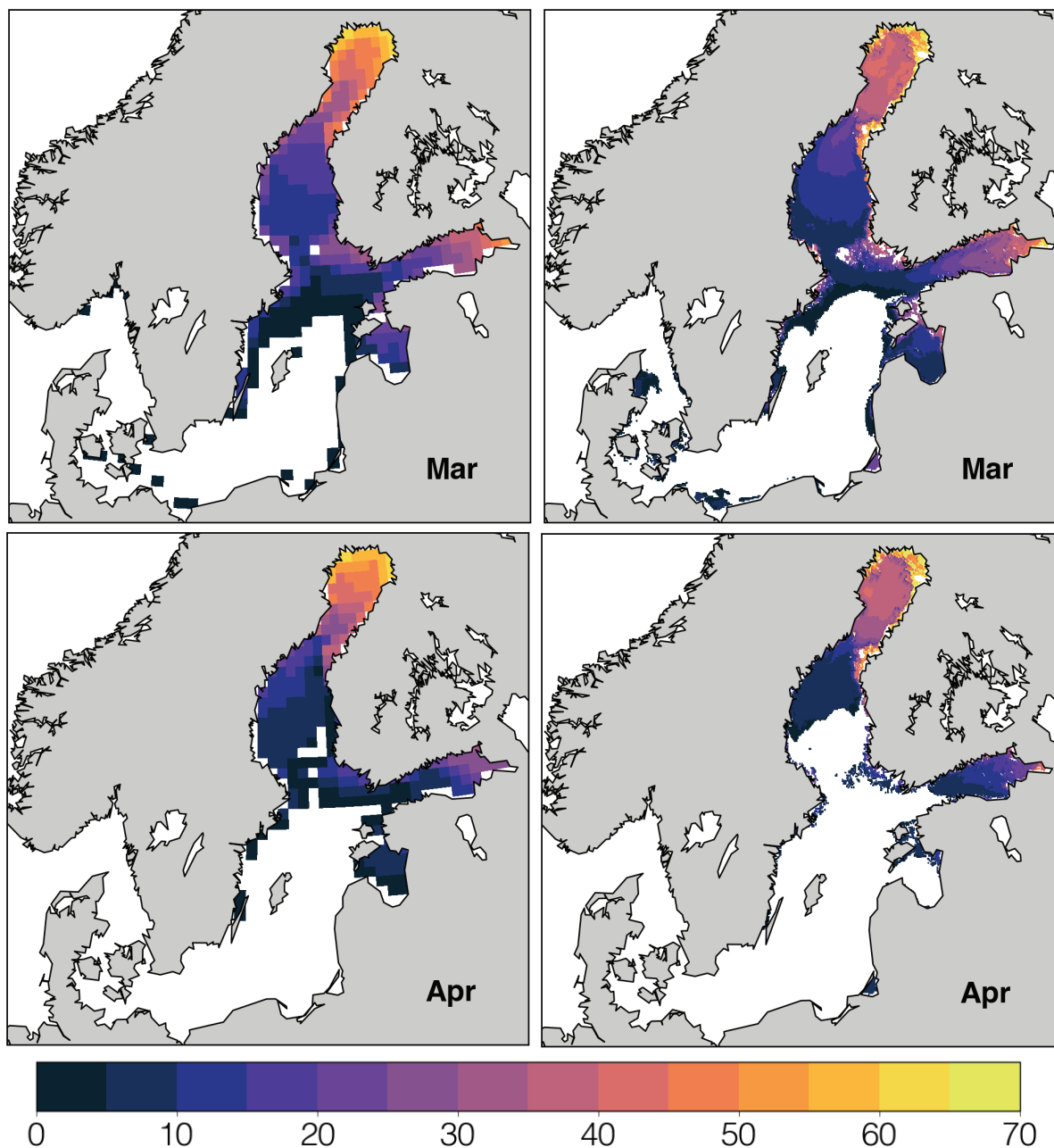
Figure 10. Same as Figure 9 but for March and April.
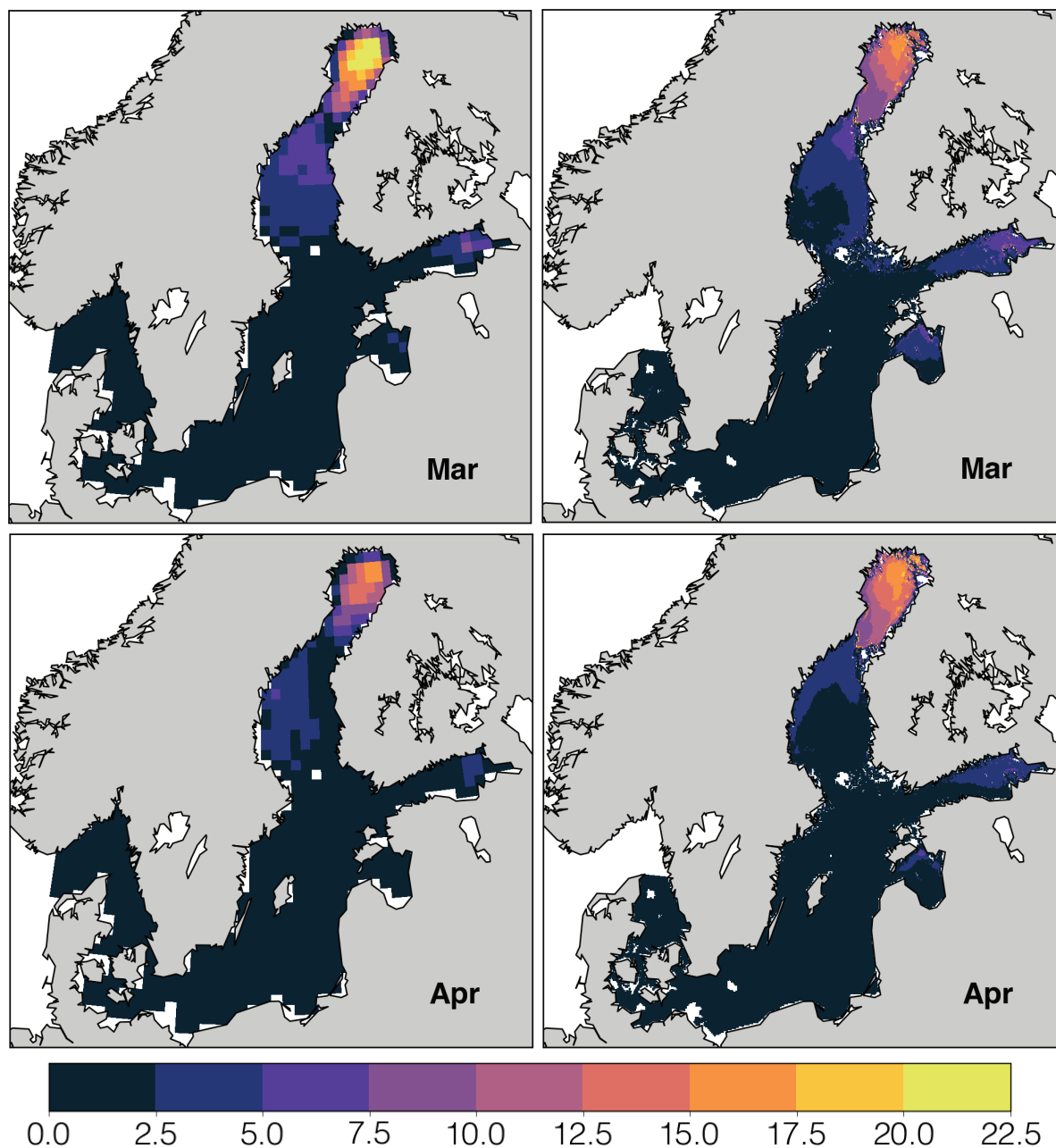
Figure 11. Climatological mean sea-ice ridge concentration in % for March and April, for the period 1961/62–1978/79. The left (right) column shows sea-ice thickness for BASIS (NEMO-Nordic). For NEMO-Nordic the sea-ice ridge concentration is estimated from the fifth ice category .
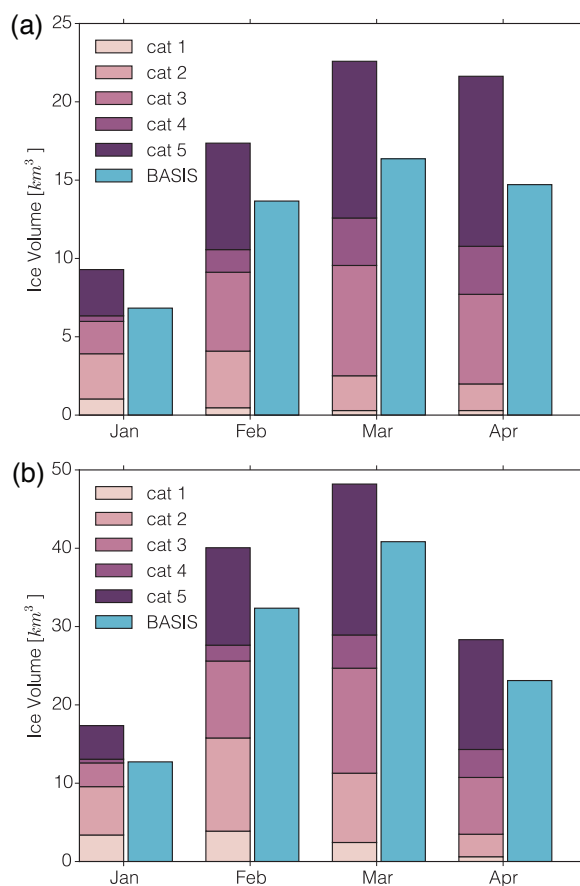
Figure 12. Climatological mean sea-ice volume for January–April, for the period 1961/62–1978/79, calculated for (a) the Bothnian Bay and (b) the entire Baltic Sea. Note that the NEMO-Nordic ice volumes are calculated for each ice category and the sum gives the total simulated ice volume.
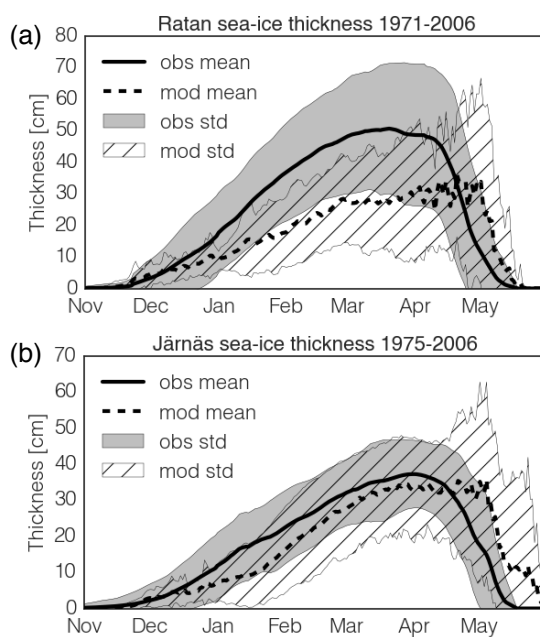
Figure 13. Seasonal simulated and observed sea-ice thickness at the coastal sites (a) Ratan and (b) Järnäs. The lines show the seasonal daily means and the filled envelopes show the ± 1 standard deviations. The seasonal cycles are calculated for the periods 1971/72–2005/06 and 1975/76–2005/06 for the Ratan and Järnäs sites, respectively. For the location of the sites see Fig. 1.
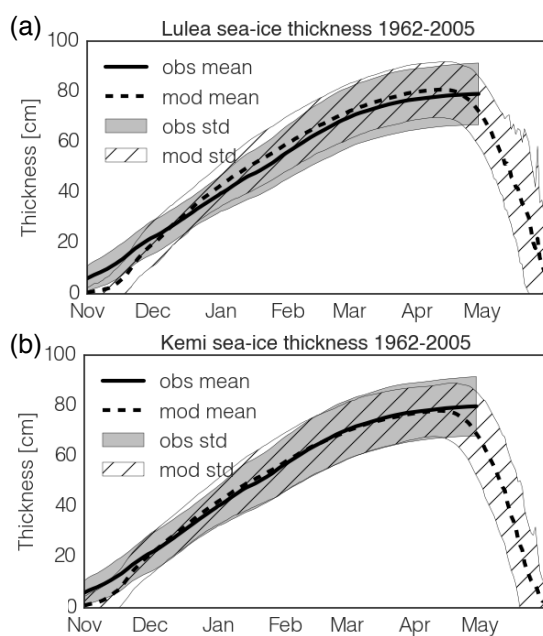
Figure 14. Seasonal simulated and freezing degree days estimated sea-ice thickness at the coastal sites (a) Luleå and (b) Kemi. The lines show the seasonal daily means and the filled envelopes show the ± 1 standard deviations. The seasonal cycles are calculated for the period 1961/62–2005/06. For the location of the sites see Fig. 1.
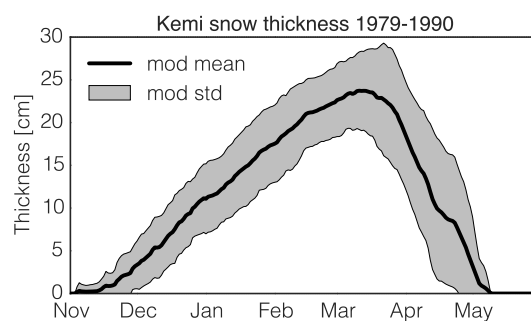
Figure 15. Seasonal simulated snow thickness at the coastal site Kemi. The black line shows the seasonal daily mean and the filled envelope show the ± 1 standard deviation. The seasonal cycle is calculated for the period 1979/80–1989/90. For the location of the Kemi site see Fig. 1.
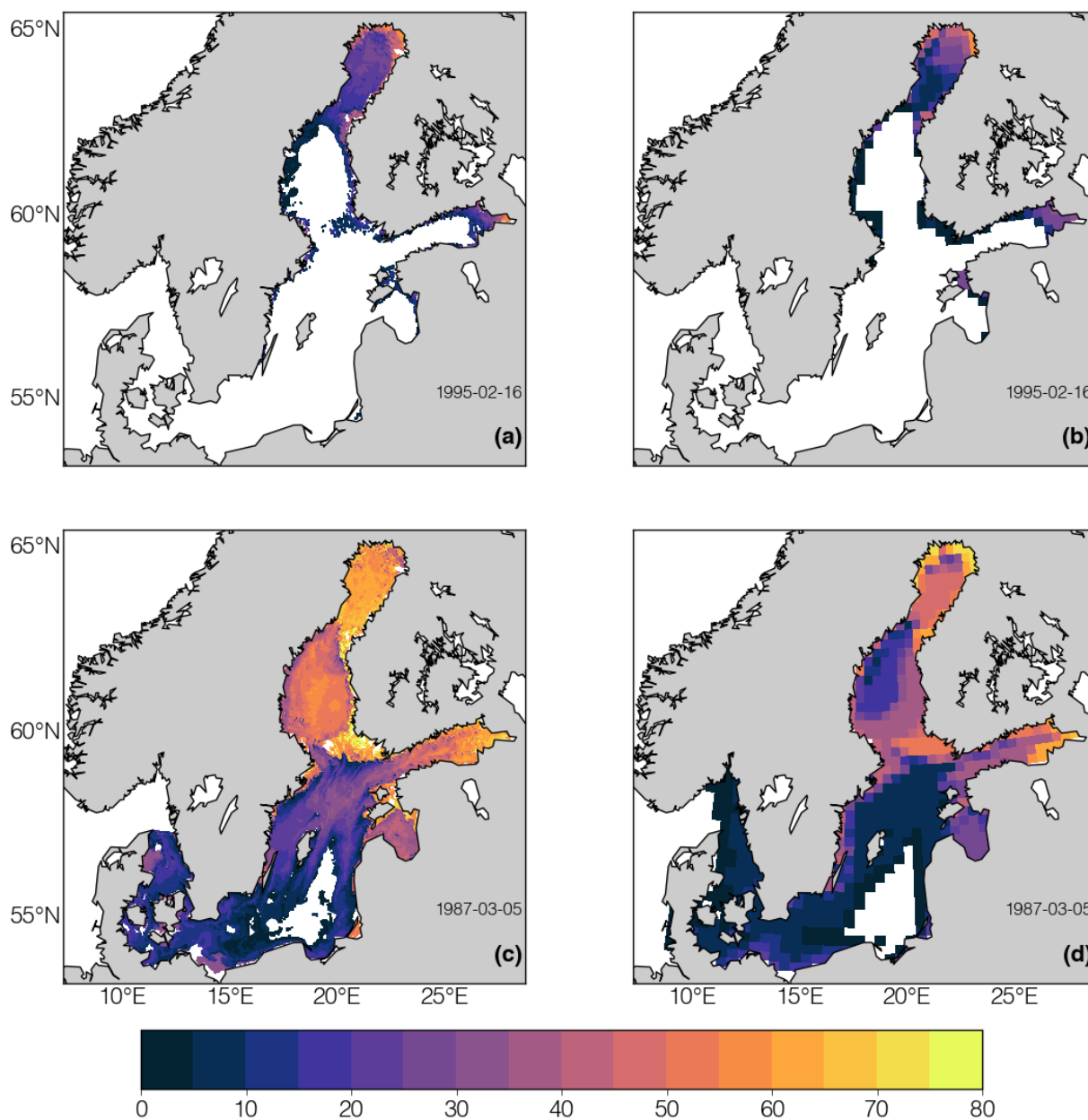
Figure 16. Daily means of level ice thickness based on IceMap data (right column) and proxy level ice thickness from NEMO-Nordic (left column) for the day of MBI for: a mild winter 1995-02-16 (upper row); and an extremely severe winter 1987-03-05 (lower row). Note that grid cells with an ice concentration lower than 15% have been masked out.

Table 1. Physical parameters in the sea ice namelist (namelist_ice_ref) that where changed in NEMO-Nordic compared to the standard global ORCA2-LIM3 that is include in the NEMO–LIM3.6 model system.

Namelist parameter	NEMO-Nordic	ORCA2-LIM3	Unit	Description
rn_hicemean	0.5	2.0	m	Expected domain-average ice thickness
rn_pstar	2.5e+4	2.0e+4	Nm^{-2}	Ice strength thickness parameter
rn_ ahi0_ref	1.0	350.0	$m^2 s^{-1}$	Horizontal sea ice diffusivity
rn_hnewice	0.01	0.1	m	Thickness for new ice formation in open water
rn_maxfrazb	0.0	1.0		Maximum fraction of frazil ice collecting at the ice base
rn_himin	0.01	0.1	m	Minimum ice thickness used in remapping
rn_betas	1.0	0.66	m	Exponent in lead-ice repartition of snow precipitation
rn_icesal	1.0e-3	4.0	$g\,kg^{-1}$	Bulk sea-ice salinity
rn_hstar	30.0	100.0	m	Determines the maximum thickness of ridged ice
rn_hraft	0.07	0.75	m	Threshold thickness for rafting